Radar-Based Mapping of the Environment: Occupancy Grid-Map Versus SAR

Timo Grebner[ID], *Graduate Student Member, IEEE*, Pirmin Schoeder[ID], *Graduate Student Member, IEEE*, Vinzenz Janoudi[ID], and Christian Waldschmidt[ID], *Fellow, IEEE*

Abstract—**For autonomous driving vehicles, highly accurate representations of the environment are essential for both trajectory planning and self-localization. Different possibilities allow to generate detailed maps of the environment based on chirp-sequence radar sensors for advanced driver assistance systems (ADASs). For the first time, this letter shows a qualitative comparison between synthetic aperture radar (SAR)- and occupancy grid map (OGM)-based environment representation using identical measurement data. The differences of existing signal processing chains as well as a visual measurement-based comparison of the resulting environmental maps is presented.**

Index Terms—**Ego-motion, frequency-modulated continuous wave (FMCW), grid maps (GMs), mapping, networks, radar systems, synthetic aperture radar (SAR).**

I. INTRODUCTION

THE increasing progress in the field of autonomous driving leads to ever higher demands on the sensor systems. With the increasing complexity of autonomous driving applications, more accurate and detailed images of the environment are required. Radar sensors offer lower costs and higher robustness in comparison to optical-based sensor systems [1]. The advantages of radar sensors stimulate the ever increasing use of radar sensors in the automotive sector [2]. In order to generate high-resolution environmental maps, new high-performance sensor architectures can be created or more information can be extracted from existing radar systems through effective signal processing [3]. The best known approach for mapping the environment with the help of radar data are grid maps (GMs), which can be classified into target list-based occupancy grid maps (OGMs) and raw data-based synthetic aperture radar (SAR) maps. Different algorithms in order to generate radar-based GMs have been presented in [4]–[6].

This letter provides for the first time a qualitative comparison between radar-based OGMs and SAR maps for creating GMs based on identical raw data using existing mapping algorithms. Especially the scenarios in which either OGM- or SAR-based mapping is advantageous are highlighted. In Section II, the basic known structures for generating GMs and for creating SAR images are presented. The measurement setup and the measurement-based comparison
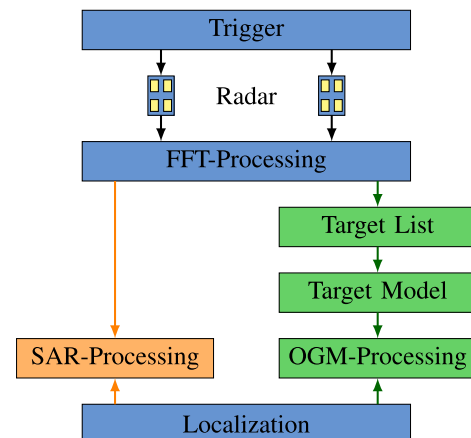
Fig. 1. Overview of the processing steps for the SAR- and OGM-based imaging based on the measurement data of $n = 2$ radar sensors.

are described in Sections III and IV. Section V summarizes the work.

II. PROCESSING CHAIN

An overview of the entire signal processing is shown in Fig. 1. The raw data of n externally triggered radar sensors is stored, processed independently, and transformed into the frequency domain using a fast Fourier transform (FFT). After the transformation into the frequency domain, a distinction between SAR processing and the generation of OGMs is made. Both OGMs and SAR images are generally cell-based representations of the environment. For advanced driver assistance systems (ADASs) using GMs to represent the environment, the distinction between occupied cells and free cells is of great relevance. OGMs and SAR images differ mainly in the resolution and the information content of each cell, but also in the signal processing of these maps. The quality of the resulting maps depends significantly on the localization and orientation accuracy of the vehicle, which is determined with high precision for the following measurement with help of a tachymeter [7].

A. Occupancy Grid Map

OGMs are generally target list-based mapping algorithms [8]. A distinction is usually made between the amplitude and OGMs, whereby the probabilistic OGM has clear robustness advantages [5]. For the generation of OGMs, the target lists are generated based on the range-Doppler information, calculated by applying a 2-D FFT on the analog-to-digital conversion (ADC) samples [9]. The relevant target

Fig. 2. Experimental system setup with two side-look radar sensors on a car.

Parameter	Value	
	S_1	S_2
Start frequency f_{start}	77.6 GHz	77.63 GHz
Bandwidth B	3.07 GHz	
Ramp repetition time T_r	67 µs	
Sampling frequency f_s (IQ)	10 MHz	
Number of ramps	384	
Number of transmitters	1	
Number of receivers	4	
Measurement rate	37 Hz	

information is extracted by using a constant false alarm rate (CFAR), subsequent peak detection, and angle of arrival (AoA) estimation. Based on these target lists, a target model as well as a sensor model is generated for each frame and each sensor [5], which can ultimately be used to generate an OGM and to update it frame by frame with [10]

$$\frac{p(m_i|z_{1:t}, x_{1:t})}{p(-m_i|z_{1:t}, x_{1:t})}$$
$$= \underbrace{\frac{p(m_i|z_t, x_t)}{1 - p(m_i|z_t, x_t)}}_{\text{current measurement}} \underbrace{\frac{p(m_i|z_{1:t-1}, x_{1:t-1})}{1 - p(m_i|z_{1:t-1}, x_{1:t-1})}}_{\text{recursive term}} \underbrace{\frac{1 - p(m_i)}{p(m_i)}}_{a\ priori\ \text{information}} \quad (1)$$

whereby $p(m_i|z_{1:t}, x_{1:t})$ describes the occupancy probability of the ith cell at time t, x the pose of the radar sensor, and z the measurement data. This allows a map update exclusively based on the current measurement including *a priori* information and the currently existing map.

B. SAR Image

In contrast to OGMs, the time-domain samples are used after applying a 1-D FFT directly for the generation of SAR maps, for which reason no target lists and no probabilistic modeling is necessary. For comparison purpose, the backprojection algorithm (BP) is used, which calculates the power of the cell m_i depending on the given sensor position x and sensor measurement z. The associated complex values of the range measurements $A_{r,k}$ are coherently projected to each grid cell resulting in complex amplitudes G [11]–[13]

$$G(m_i|z_{1:t}, x_{1:t})$$
$$= G(m_i|z_{1:t-1}, x_{1:t-1})$$
$$+ \sum_{k=1}^{K} A_{r,k}(m_i|z_{t_k}) \cdot \exp\left(-j2\pi \frac{f_{\text{start}}}{c_0} \cdot 2r(m_i|x_{t_k})\right). \quad (2)$$

To ensure a proper comparison, frame-based radar sensors are used for the evaluation, whereby t is discretized to the frame rate, t_k represents the time stamps of the individual K ramps, and r is the distance. In contrast to OGM, SAR does not accumulate probabilities p in each cell but complex amplitudes G representing the reflected power.

III. MEASUREMENT SETUP

The measurement setup used for evaluating the presented methods is shown in Fig. 2 and consists of two incoherently operated distributed chirp sequence radar sensors. A trigger is

Fig. 3. Photograph of the measurement scene with several parked cars, hedges and trees, fences, roads, and gravel car parks. Approximated trajectory in red.

used to synchronize the radar sensors in the network to avoid interference. A small shift in the carrier frequency of the radar sensors prevents interference between them. The sensors are arranged in such a way that the lateral areas, relevant for SAR, are illuminated, and a large field of view (FoV) is covered. The radar parameters are listed in Table I.

The measurement was performed along a rectilinear trajectory $[(0, 0) \rightarrow (128, 0)]$ m with a speed up to 15 ms^{-1} on a parking lot, where numerous parked cars as well as other obstacles such as fences, lanterns, and trees exist as shown in Fig. 3.

IV. MEASUREMENT RESULTS

For reasons of comparability, the same measurement data were used to calculate OGM- and SAR-based maps with a pixel size of 1 cm. The result after SAR processing is shown in Fig. 4(a), and the result of OGM in Fig. 4(b). Significant differences in detectability, resolution, and identifiability can be observed, as explained in Sections IV-A–IV-C.

A. Detectability

Targets with a high RCS, such as street lamps or cars, as well as low radar cross section (RCS) targets with large surface area, such as hedges and trees, can be clearly detected in both representations and distinguished from the free space. This is in contrast to low RCS targets with small surface areas such as the fence, which is only visible in the SAR-based image.

In the SAR image, Fence 1 and Fence 2 can be recognized as a continuous obstacle, whereas in the OGM only the posts of the fence are visible. These wrongly detected free spaces of about 2 m can be problematic and lead to unsafe trajectory planning. Here, the SAR processing of the raw data clearly provides robustness advantages.
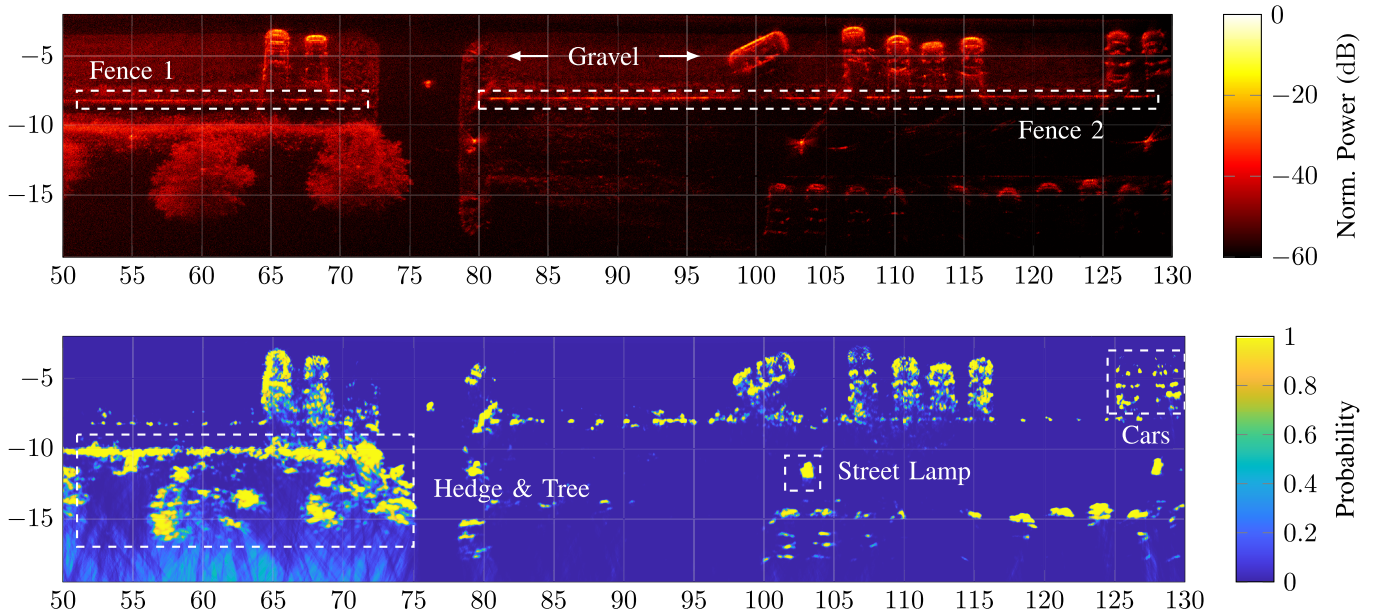
Fig. 4.   Comparison of SAR-based (top) and OGM-based (bottom) mapping methods of a car park with vehicles, street lights, hedges and trees, and fences. x- and y-axes are in meters.
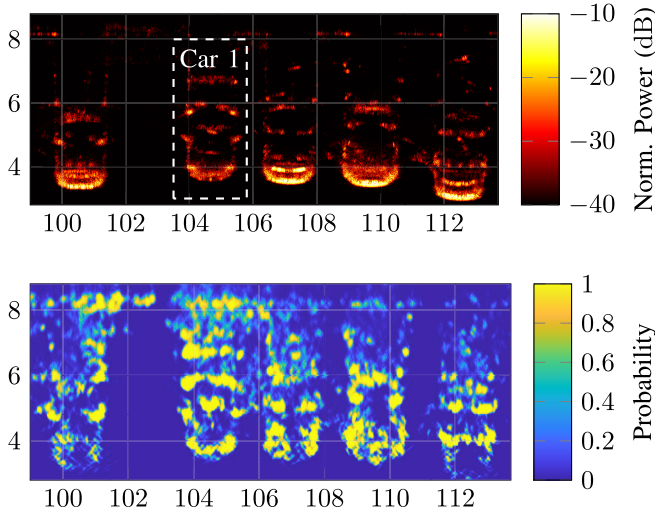

Fig. 5.   Detailed comparison of parked cars for SAR-processed image (top) and OGM-based representation (bottom). x- and y-axes are in meters.

B. Resolution and Accuracy

The contour of all targets in the SAR image is clearly more detailed and focused. The individual branches of the trees as well as the vehicle contours can be mapped more precisely, which is especially valid for targets with many scattering centers. Therefore, even individual branches of the trees can thus be captured in detail, also inside the tree crown.

In addition, the resolution strongly depends on the synthetic aperture size, which can be observed from the marked cars. At the end of the trajectory at (128,0) m and thus the reduced synthetic aperture, the cars marked in the OGM are mapped worse and can no longer be identified or clustered as such,

while for the SAR image, a short aperture is sufficient to map them in detail.

C. Additional Information

Due to different processing steps, the SAR image is power-dependent, which results in objects at a greater distance and lower RCS being represented more faintly. As soon as it is a matter of identifying surrounding areas, such as asphalt or gravel, this is only possible to a limited extent with an OGM due to the probabilistic state description. While the OGM represents all grounds, such as asphalt or gravel, as "Free-Space," the SAR image can clearly resolve between the road and the gravel path on which the vehicles are parked.

Likewise, the resolution of the OGM is not sufficiently high to depict objects in detail, which can be seen in Fig. 5 (top and bottom). While only point clouds are recognizable in the OGM, the contour of the car can be identified visually in the SAR image. Furthermore, Fig. 5(a) shows that only one car is parked with the cowl facing forward, as both the side mirrors and the rear-view mirror can be seen.

V. CONCLUSION

For the first time, a qualitative comparison between SAR- and OGM-based mapping results could be made based on identical measurement data. The advantages of OGM-based maps are mainly the robustness with respect to false detections and measurement inaccuracies. Moreover, the occupancy status of each cell is directly determinable from the cell amplitude. SAR mapping is much more computationally expensive due to the ramp-by-ramp update step. However, SAR provides much more accurate images of the environment, which ultimately enables the detection of even small details as well as street conditions. Moreover, due to raw data processing, SAR images are independent of pre-segmented target lists.

REFERENCES

[1] F. Roos, J. Bechter, C. Knill, B. Schweizer, and C. Waldschmidt, "Radar sensors for autonomous driving: Modulation schemes and interference mitigation," *IEEE Microw. Mag.*, vol. 20, no. 9, pp. 58–72, Sep. 2019.

[2] C. Waldschmidt, J. Hasch, and W. Menzel, "Automotive radar—From first efforts to future systems," *IEEE J. Microw.*, vol. 1, no. 1, pp. 135–148, Jan. 2021.

[3] M. Gottinger *et al.*, "Coherent automotive radar networks: The next generation of radar-based imaging and mapping," *IEEE J. Microw.*, vol. 1, no. 1, pp. 149–163, Jan. 2021.

[4] K. Werber *et al.*, "Automotive radar gridmap representations," in *IEEE MTT-S Int. Microw. Symp. Dig.*, Apr. 2015, pp. 1–4.

[5] P. Hugler, T. Grebner, C. Knill, and C. Waldschmidt, "UAV-borne 2-D and 3-D radar-based grid mapping," *IEEE Geosci. Remote Sens. Lett.*, vol. 19, pp. 1–5, 2022.

[6] M. Steiner, T. Grebner, and C. Waldschmidt, "Millimeter-wave SAR-imaging with radar networks based on radar self-localization," *IEEE Trans. Microw. Theory Techn.*, vol. 68, no. 11, pp. 4652–4661, Nov. 2020.

[7] *Trimble Universale Totalstation SPS930*, Trimble, Sunnyvale, CA, USA, 2018.

[8] S. Thrun, "Learning metric-topological maps for indoor mobile robot navigation," *Artif. Intell.*, vol. 99, no. 1, pp. 21–71, Feb. 1998.

[9] V. Winkler, "Range Doppler detection for automotive FMCW radars," in *Proc. Eur. Radar Conf.*, Oct. 2007, pp. 1445–1448.

[10] S. Thrun, "Learning occupancy grids with forward models," in *Proc. IEEE/RSJ Int. Conf. Intell. Robots Syst. Expanding Societal Role Robot. Next Millennium*, vol. 3, Oct./Nov. 2001, pp. 1676–1681.

[11] J. C. Curlander and R. N. Mcdonough, *Synthetic Aperture Radar: Systems and Signal Processing*. New York, NY, USA: Wiley, 1991.

[12] O. Frey, C. Magnard, M. Ruegg, and E. Meier, "Focusing of airborne synthetic aperture radar data from highly nonlinear flight tracks," *IEEE Trans. Geosci. Remote Sens.*, vol. 47, no. 6, pp. 1844–1858, Jun. 2009.

[13] L. M. H. Ulander, H. Hellsten, and G. Stenström, "Synthetic-aperture radar processing using fast factorized back-projection," *IEEE Trans. Aerosp. Electron. Syst.*, vol. 39, no. 3, pp. 760–776, Jul. 2003.